Cooperative Switching in Large-Area Assemblies of Magnetic Janus Particles

Sangyeul Hwang, Trung Dac Nguyen, Srijanani Bhaskar, Jaewon Yoon, Marvin Klaiber, Kyung Jin Lee, Sharon C. Glotzer,* and Joerg Lahann*

Magnetic Janus particles (MJPs) have received considerable attention for their rich assembly behavior and their potential technological role in applications ranging from simple magnetophoretic displays to smart cloaking devices. However, further progress is hampered by the lack of predictive understanding of the cooperative self-assembly behavior of MJPs and appropriate dynamic control mechanisms. In this paper, a detailed experimental and theoretical investigation into the magnetically directed spatiotemporal self-assembly and switching of MJPs is presented. For this purpose, a novel type of MJPs with defined hemispherical compartments carrying superparamagnetic iron oxide nanoparticles as well as a novel simulation model to describe their cooperative switching behavior is established. Combination of the theoretical and experimental work culminates in a simple method to direct assemblies of MJPs, even at high particle concentrations. In addition, a magnetophoretic display with switchable MJPs is developed on the basis of the theoretical findings to demonstrate the potential usefulness of controlled large-area assemblies of magnetic Janus particles.

Dr. S. Hwang, Prof. T. D. Nguyen,[+] Prof. K. J. Lee, Prof. S. C. Glotzer, Prof. J. Lahann
Department of Chemical Engineering
University of Michigan
2300 Hayward St., Ann Arbor, MI 48109, USA
E-mail: sglotzer@umich.edu; lahann@umich.edu

Dr. S. Hwang, Dr. J. Yoon, Prof. K. J. Lee, Prof. S. C. Glotzer, Prof. J. Lahann
Biointerfaces Institute
University of Michigan
2300 Hayward St., Ann Arbor, MI 48109, USA

Dr. S. Bhaskar, Dr. J. Yoon, Prof. J. Lahann
Macromolecular Science and Engineering
University of Michigan
2300 Hayward St., Ann Arbor, MI 48109, USA

M. Klaiber, Prof. J. Lahann
Institute for Functional Interfaces
Karlsruhe Institute of Technology
Hermann-von-Helmholtz-Platz 1, 76344 Eggenstein-Leopoldshafen, Germany

Prof. S. C. Glotzer
Department of Physics
University of Michigan
2300 Hayward St., Ann Arbor, MI 48109, USA

Prof. S. C. Glotzer
Department of Applied Physics
University of Michigan
2300 Hayward St., Ann Arbor, MI 48109, USA

The ORCID identification number(s) for the author(s) of this article can be found under https://doi.org/10.1002/adfm.201907865.

[+]Present address: Department of Chemical and Biological Engineering, Northwestern University, Evanston, IL 60208, USA

1. Introduction

Materials are typically characterized by a permanent set of properties, such as color, hydrophilicity, or surface texture. However, examples of reversible switchable materials exist, including those with important scientific and technological implications. Reversible switching of the orientation of liquid crystal (LC) polymers with electric fields forms the foundation of modern LC displays and the electrophoretic switching of pigments has resulted in electrophoretic displays.[1,2] In typical reversibly switchable materials, two or more stable states are present and toggling between these states is classically triggered by the application of a defined stimulus, such as an electrical field.[3–6] Although the vast majority of these switches exploit electric fields, alternate stimuli, such as magnetic fields, can also drive surface switching.[7,8] In the past, the use of magnetic fields for surface switching has been hampered by the lack of suitable anisotropic transduction units and simple cooperative manipulation of large-area assemblies.[9]

Magnetic Janus particles (MJPs) with precisely patterned surfaces have been the focus of recent research because of their potential for synchronized self-assembly.[10–12] Although major progress has been made with respect to the fabrication of MJPs,[9,13–15] predictive understanding of their cooperative self-assembly behavior in magnetic fields as well as the development of dynamic control mechanisms remain emerging fields of research.[9,14,16] Complexity in such studies originates primarily from magnetic patterns on the surface of particles.[9,17]

Previous studies on optomagnetic[9] or magnetic[14,18] trapping demonstrated accurate controllability of individual MJPs, but the controlled switching of larger assemblies of MJPs has remained an continuous challenge, because it requires a balanced interplay between the magnetic forces induced by the external magnetic field and the magnetic dipole interactions between individual MJPs.[19] Building on these studies, we now designed and prepared novel types of bicompartmental magnetic MJPs, where the magnetic component is localized within a hemispherical compartment, rather than being deposited as a surface patch. Only the hemispherical compartment of the particles is magnetically active (**Figure 1**). Moreover, we developed a simulation model to gain further insights into magnetically directed spatiotemporal self-assembly and switching of MJP, and experimentally studied their switching.
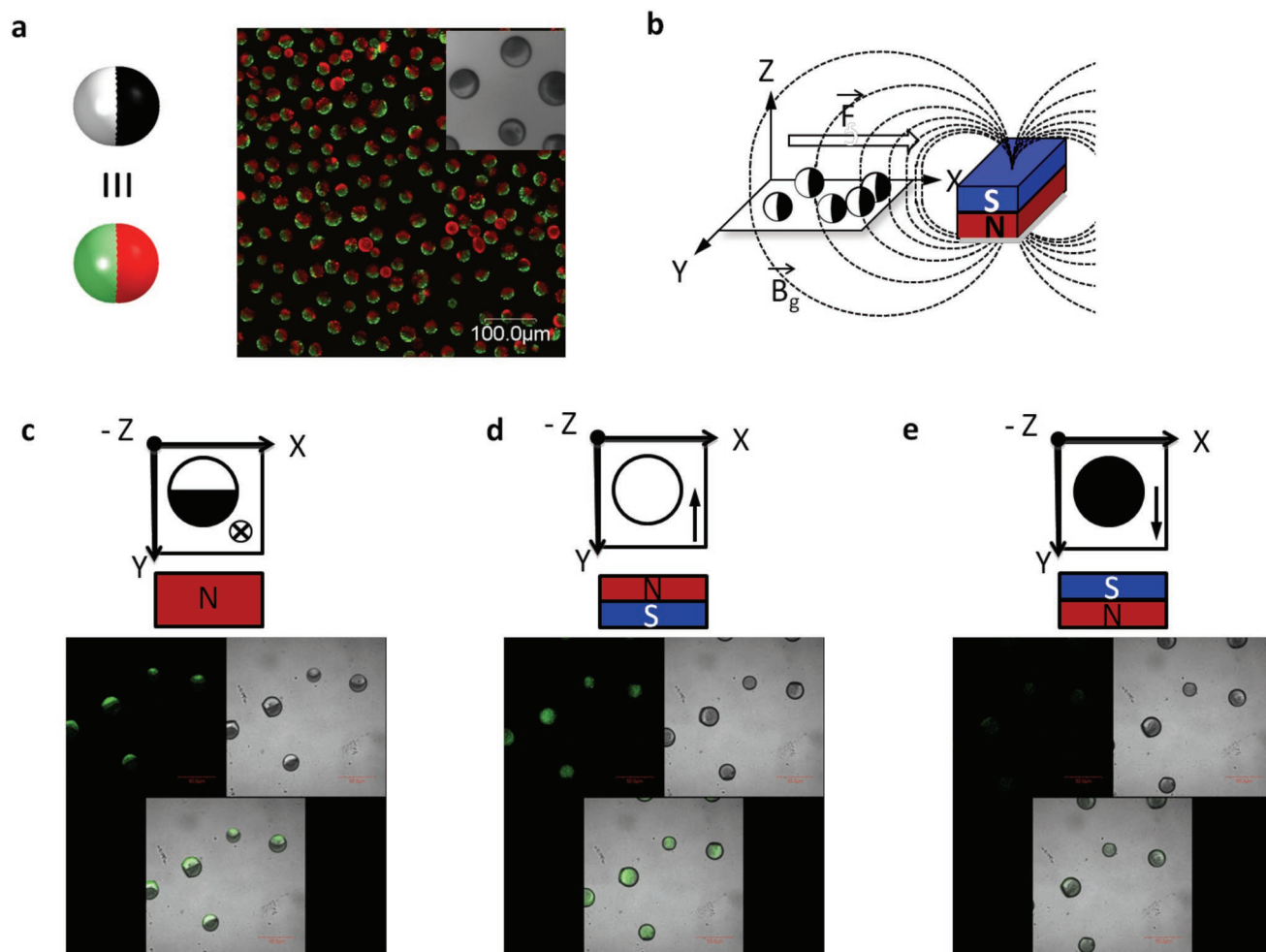
Figure 1. Synchronized cooperative switching of magnetic Janus particles (MJPs). a) A scheme of MJPs and the images obtained by confocal laser scanning microscopy (CLSM) and optical microscopy (OM); where magnetic and nonmagnetic compartments are encoded by red- and green-colored fluorescence, and the magnetic compartment appeared to be darker. b) Experimental configuration with the MJPs sitting in a microscopic cover-glass and the single magnet with perpendicular field direction to the x–y-plane. c–e) Experimental setup and corresponding CLSM micrograph (FITC channel at the left, transmitted light at the right, and superimposed at the bottom) with a low concentration of MJPs (bottom view, −z).

2. Results and Discussion

The combined theoretical and experimental work culminates in a simple method to direct various assemblies of MJPs, even at high concentrations. Finally, to demonstrate wider applicability, a simple magnetophoretic display was developed from compartmentalized MJPs on the basis of the theoretical findings.

An example of an assembly of MJPs is shown in Figure 1. Experimentally, all MJPs were prepared by electrohydrodynamic (EHD) co-jetting.[18,20] This method allows for preparing a wide range of different multicompartmental particles with diverse compartmentalization, compositions, and shapes.[20–23] The polymer particles (10–25 μm in diameter) were composed of one compartment (i.e., one hemisphere) that included magnetite nanocrystals (Fe$_3$O$_4$, 28 nm in diameter) and a red fluorophore and a second compartment containing a green fluorescent dye (Figure 1; Figure S1, Supporting Information). The confocal laser scanning micrograph (CLSM) shown in Figure 1a confirms the exquisite compartmentalization within

the MJPs. The particles responded to an applied magnetic field by synchronous movement reflecting on the reduced rotational degree of freedom imparted by their unique bicompartmental design.

In parallel, we developed a simulation model for self-assembly and switching of MJPs (**Figure 2**). Our theoretical study employed molecular dynamics simulations of a phenomenological particle-based model of MJPs (Figure 2a). Our model assumed the MJPs to be translationally constrained within the x–y-plane with periodic boundary conditions applied to the y-direction. The magnetic field was parallel to the z-axis and increased in strength along the positive direction of the x-axis. Using the energy scale of μB, where μ is the MJP magnetic dipole moment and B is the magnetic field, we defined the dimensionless magnetic dipole moment as $m = \mu/k(\sigma^3 \mu B)^{1/2}$ and the dimensionless gradient strength $g_B = 4a\pi(\sigma^5/\mu B)^{1/2}/\mu k$, where a is the actual gradient strength in ≈1.0 T m^{-1} and k is a scaling factor used for matching simulation with experimental kinetics (see the Experimental Section and the Supporting Information).
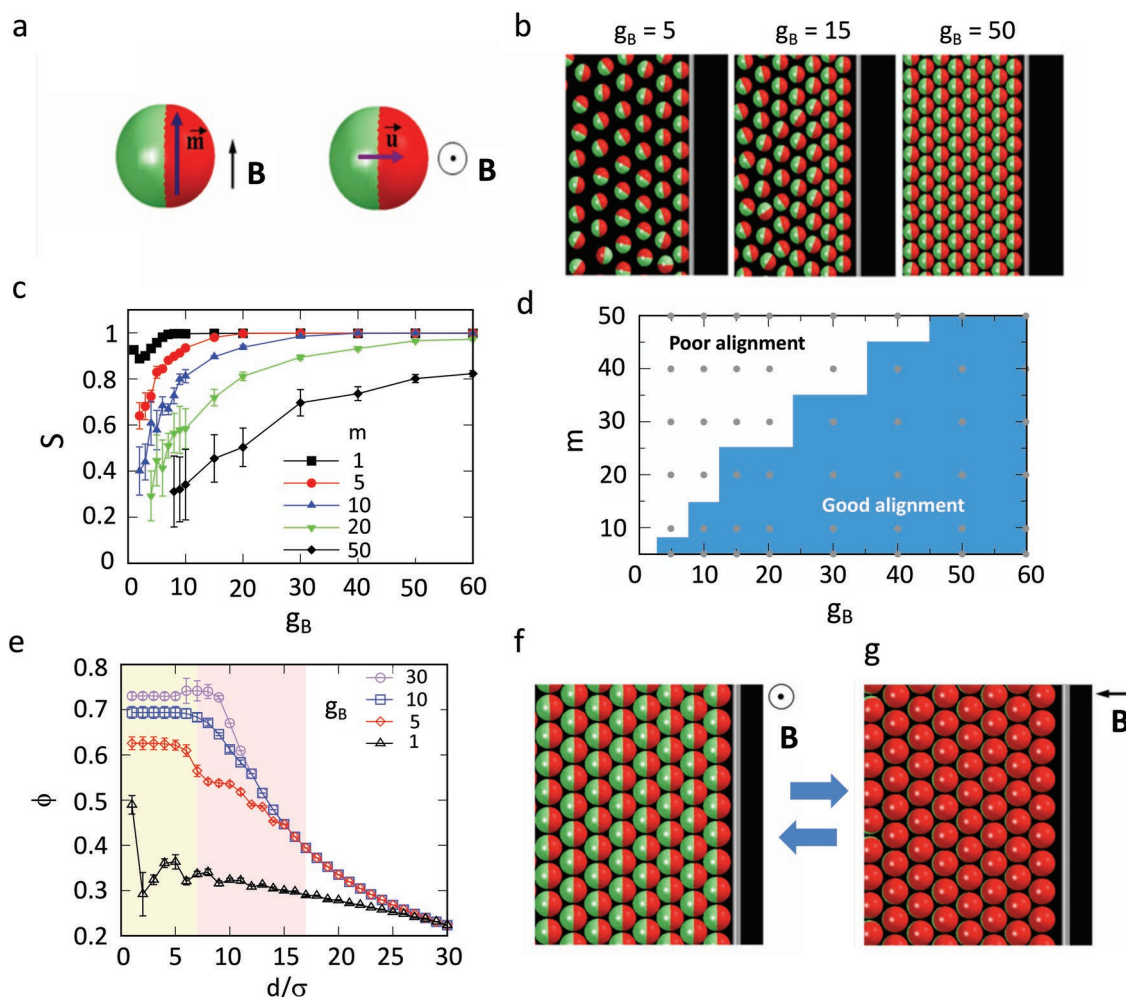
Figure 2. Simulation model and results. a) Model Janus particles: Left: side-view; right: top-view; **m**: magnetic dipole vector; **u**: orientational unit vector. b) Snapshots for systems with different gradient strengths (g_B) with a given particle magnetic dipole $m = 10$. c) Alignment order parameter $S(\mathbf{u})$ as a function of the gradient strength (g_B) and particle magnetic dipole (m). Error bars are obtained from 12 independent runs. d) Phase diagram summarizing the alignment of the particles with the magnetic field as a function of m and g_B: "good alignment" corresponds to $S > 0.8$; "poor alignment" corresponds to $S < 0.6$. The dots are the simulated state points. e) Local packing density (ϕ) with different gradient strengths with $m = 10$. Error bars are obtained from 10 independent calculations from each sample. f,g) Reconfigurable assembly: f) close packing assembly with the gradient field perpendicular to the plane and g) the field rotation to be in-plane resulting in the magnetized compartments to face into the page. Reconfigurability is induced when the field is rotated back and forth.

As visually revealed by Figure 2b, upon increasing the gradient strength from $g_B = 5$ to $g_B = 50$ with $m = 10$, corresponding to the experimental range of parameter values, the packing arrangement of the simulated MJPs correlated well with those used for the experimental studies.

To quantify the overall alignment of MJPs, we define an order parameter S as

$$S = \left\langle \frac{1}{N} \sum_{i}^{N} \mathbf{u}_i \cdot \mathbf{x} \right\rangle \quad (1)$$

where $\mathbf{u}_i$ is the unit vector characterizing the particle orientation, $\mathbf{x}$ is the unit vector of the x-axis, and the average is performed over 12 independent runs. S varied from zero to unity, equivalent to a random distribution of the alignment vector to a perfect alignment, respectively.

The particle alignment was poor ($S < 0.8$) in the range of small g_B and large m (Figure 2c). The notable fluctuation in S indicated that the field gradient is insufficient for directing the particle assembly within these limits. As m increased, the minimum value of g_B required to have good alignment also increased. To yield a degree of alignment of $S > 0.9$, g_B must be greater than 15.0 for $m = 5$ and greater than 60.0 for $m = 15$. However, we noted that if g_B is too high relative to m, kinetic effects due to the large magnetic force caused a significant decrease in the particle alignment. Consequently, the expected ordered assembly of the MJPs with minimal potential energy may not be achieved in practice under these extreme conditions. We summarize the particle alignment order as a function of m and g_B into a phase diagram shown Figure 2d.

The local density (ϕ) measured by $\phi = N\pi\sigma^2/4A$, where N and A are the number of particles and surface area local to the

**ADVANCED
SCIENCE NEWS**
www.advancedsciencenews.com
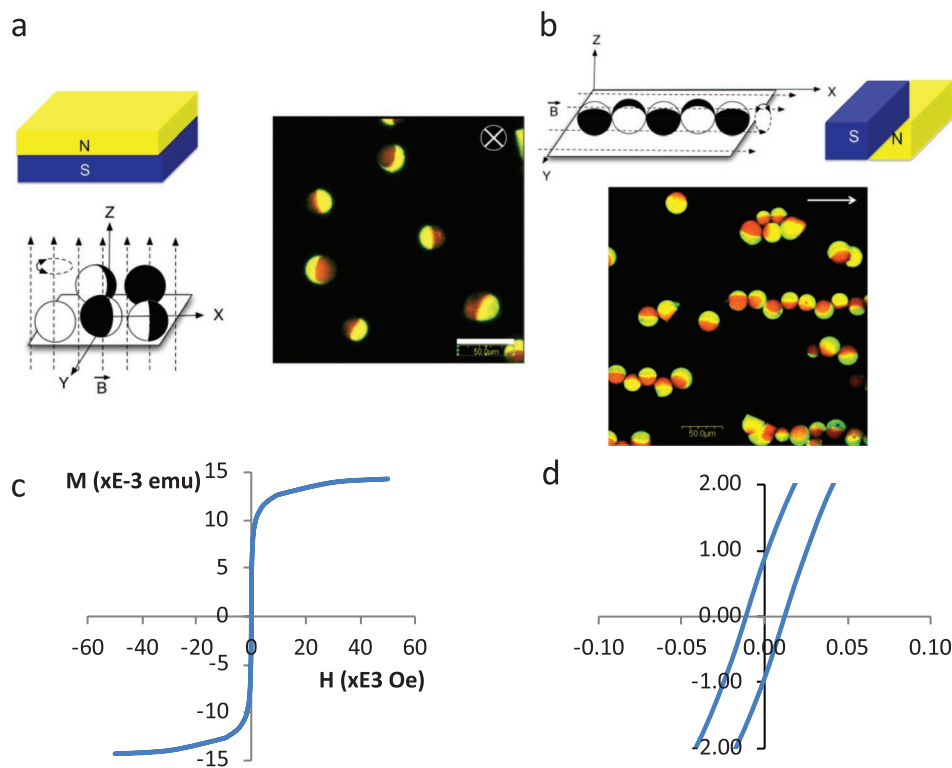
**ADVANCED
FUNCTIONAL
MATERIALS**
www.afm-journal.de

Figure 3. Assemblies of magnetic Janus particles. The different assemblies of MJPs depend on the magnet position and the field direction, where **B** is a magnetic field gradient. a) The repulsive MJPs due to the parallel orientation of the induced dipole caused by the magnet located at the Z position parallel to the field direction (z-axis), where an experimental configuration is at the left side and the corresponding CLSM image at the right side. b) Staggered chains form from MJPs if assembled by a magnet placed on the x–y-plane with the parallel field direction (x- or y-axis), where a schematic experiment figure is at the top and the corresponding CLSM image at the bottom. c) M–H hysteresis of the particles measured by a SQUID magnetometer (Quantum Design) at room temperature. d) An enlarged image of (c) near the center area, showing that the coercivity is close to zero.

vicinity of interest, respectively, is another measure to systematically analyze the assemblies of the MJPs in our simulations (Figure 2e). Under the influence of a weak gradient ($g_B = 1$), the particle density was low and their orientation is relatively random except for the first row where the field was the most influential. For higher field gradients ($g_B = 5$, 10, and 30), the density profile exhibited three distinct regions as color coded in Figure 2e. The darker area on the left corresponds to a state where the gradient field dominated the packing of the particles, leading to a plateau region of particle density, which was broadened and shifted to higher values with increasing g_B. In the intermediate region, the competition between the field strength and particle repulsion strength led to a gradient in particle density. In the rightmost domain, the particles assembled into a sparse triangular array as the gradient field became weaker than the strong dipole–dipole repulsion, causing a gradual decrease in the local density.

Figure 2f shows the close-packed structure with the field perpendicular to the x–y-plane obtained by simulation ($g_B = 10$, $m = 5$). As the field vector **B** was rotated by 90° to face the x–y-plane, the particles rotated orthogonally so that their induced magnetic dipoles aligned with the magnetic field (Figure 2g). These findings agreed well with our experimental results (Figure 4g). The dynamic rotation of the MJPs completed within a second, nearly equal to the time to rotate the field. In our simulation,

with a step change in the direction of **B**, the system completed the switching almost immediately, i.e., within 100 simulation time steps, corresponding to ≈0.01 s. We note that Figure 2g is not the ground state with the in-plane field, but rather a stable kinetic trap allowed by both the initial configuration (Figure 2f) and the gradient field. This state remained stable during the experiment, in agreement with simulation, i.e., for about 10^7 time steps. The simulation model reproduced our experimental results well (**Figure 3** in conjunction with Figure S2 in the Supporting Information).

As expected, MJPs assembled into a staggered chain to minimize the energy of the induced dipole interactions, when a magnetic field is placed parallel to the x–y-plane (Figure 3a,b).[11] We further observed that MJPs exhibited close-to-ideal superparamagnetic responses (Figure 3c,d). When the field was perpendicular to the x–y-plane, the longitudinal direction of the magnetic compartment of the MJPs oriented along the z-direction due to their magnetic shape anisotropy.[24] Because the induced magnetic dipoles were parallel to the z-axis, their interactions were repulsive[25,26] and the particles did not aggregate; even at high particle concentrations (Figure 3). Still, the rotational freedom in the z-direction led to a random orientation of the magnetite compartments along the z-axis. These findings differ from the behavior observed for the case that the direction of the magnetic field is perpendicular to the surface
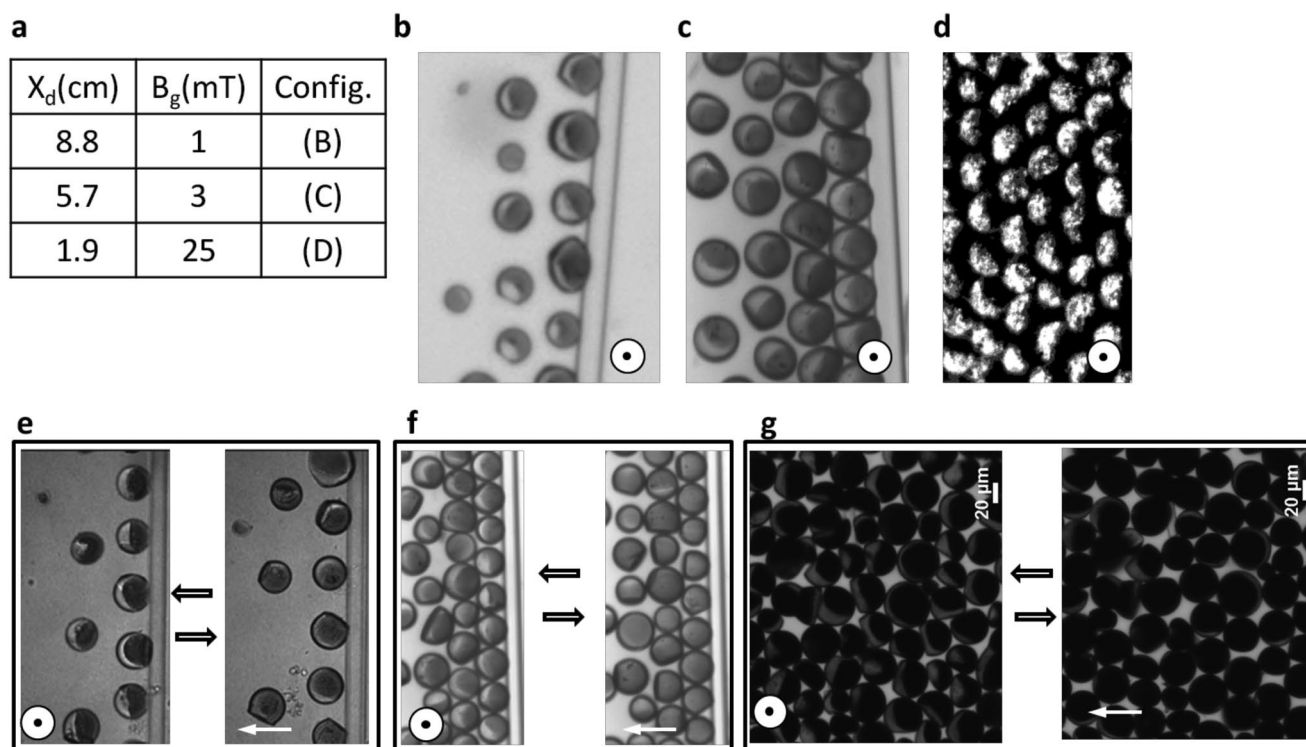
Figure 4. Spatiotemporal self-assembly of MJPs directed by a gradient field and their reconfigurable synchronization by a rotational field. a) The measured magnetic field at three different distances between the magnet and 1D barrier (PLGA fiber) (refer to Figure 1b), and the results in three states of MJPs. b) OM micrograph showing a low packing density of the MJPs at 1 mT, while the orientation of all the MJPs faces toward the PLGA fiber. c) OM image exhibiting a gradient density of the MJPs with partial contacting from the wall at 3 mT. d) OM reflective image showing a hexagonal close-packing with the specified orientation of the MJPs under 25 mT. e–g) Two sets of OM images for reconfigurable synchronization of MJPs by orthogonally rotating the field gradient at e) low density, f) gradient density, and g) close packed, respectively.

(Figure 1). Simply positioning the magnetic field perpendicular to the plane of self-assembly (Figure 1b) induced the dipole moments of the superparamagnetic nanoparticles encapsulated in the MJPs to orient along the z-axis. In this configuration, the magnetic compartments must repel each other. The presence of a magnetic field gradient caused the magnetic compartments of the MJPs to rotate due to a difference in potential energy between magnetic and nonmagnetic compartments. In this geometry, the orientation of the MJPs should be synchronized. Consequently, Figure 1c reveals cooperative harmonization and alignment of the magnetic compartments of the MJPs. The magnetic compartments (red) oriented with the perpendicular magnetic field (Figure 1c–e). Our experimental findings matched the simulation results with high fidelity and revealed the interplay between the dipole repulsion among MJPs and the field gradient with regards to the assemblies' structural and reconfigurable properties.

The applied magnetic field gradient (B_g) decreased with the distance from the wall. **Figure 4**a reveals this trend for the B_g values equivalent to the dimensionless gradient strengths $g_B = 5$, 15, and 50 with $m = 10$ (see also Figure 2b). If the magnetic force (**F**) exceeded the drag force, the MJPs translated and rotated to allow the magnetic compartments to orient into the external magnetic field gradient. Eventually, the translating particles were forced to jam by virtue of an internal barrier in the form of a PLGA fiber (20 μm in diameter) placed normal to

the magnetic field direction. At the barrier, the jammed MJPs aligned into distinct rows. Because of the repulsion between parallel magnetic dipoles, the MJPs assumed defined distances from each other, while maintaining the orientation of the magnetic compartment (Figure 4b). Increasing the magnetic field gradient caused the particles near the wall to arrange in a hexagonally close-packed configuration, whereas particles farther away from the wall were packed less densely (Figure 4c). Eventually, MJPs experiencing a dimensionless gradient strength above $g_B = 50$ assumed a hexagonally closed packing, which is in good agreement with our simulation results (Figure 4d). Moreover, the self-assembled MJPs populations underwent synchronized switching in response to a rotational field. We noted that the switching is independent of the MJP density (Figure 4e–g).

With the basic theoretical and experimental framework in hand, we next demonstrated a simple optical display configuration based on magnetophoretic self-assembly, which featured optical color changes observable with the bare eye (**Figure 5**; Movie S1, Supporting Information). We first prepared larger MJPs to match the approximate size of individually observable pixels. In addition, it was deemed critical to ensure that both colored compartments were identical in size. Rather than directly preparing compartmentalized particles via electrohydrodynamic co-jetting,[27] bicompartmental magnetic microcylinders (Figure 5b) with sizes of ≈450 μm in diameter and
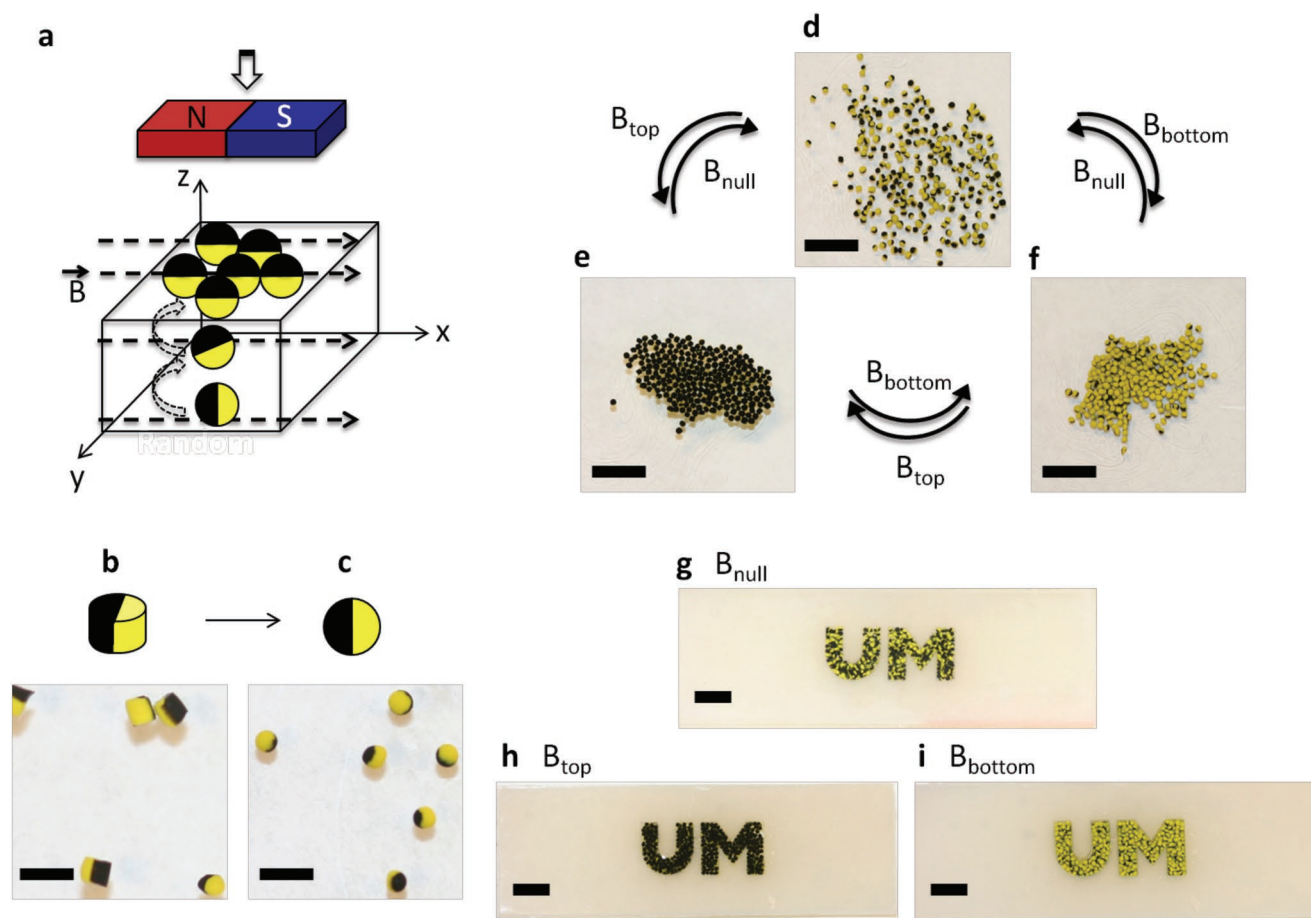
Figure 5. Design of a simple magnetophoretic display. a) A scheme for 2D alignment of MJPs by applying a magnetic field gradient on top of a vessel (z-axis) with an orthogonal field direction parallel to the x–y-plane. b) Bicompartmentalized magnetic microcylinders (diameter and height are 400–450 µm, black) manufactured by EHD co-jetting and microsectioning.[28] c) Magnetic Janus microspheres prepared from microcylinders by shape transformation. d) Randomly located spherical MJPs in the absence of magnet (B_{null}). e) 2D alignment of spherical MJPs showing a black color as the magnet located at the top of vessel (B_{top}). f) A yellow color appearing as the magnet located at the bottom of vessel (B_{bottom}). Magnetically switchable display in the form of "UM" letters colored from g) random to h) black and i) yellow states depending as a function of the position of the magnet (Movie S1, Supporting Information). Scale bars: b,c) 0.9 mm and d–i) 4.0 mm.

length were prepared by combining the electrospinning of EHD co-jetting and automated microsectioning (see the Experimental Section).[28] We note that there is a tradeoff between the rotational velocity which increases with decreasing particle diameter, and the requirement of a sufficiently large particle size (optical pixel) that is discernible by the naked human eye. These microcylinders featured two distinctive optical colors, black (magnetite and carbon black) and yellow (yellow pigment), separately incorporated into each compartment. The microcylinders were then transformed into spheroids (≈450 µm in diameter) by applying 1,4-dioxane as a plasticizer in an aqueous suspension (see the Experimental Section and Figure 5c).[29] The individual compartments of the particles were still clearly distinguishable, even after shape-shifting.

Spherical MJPs were randomly placed in a solution of Tween 80 and ethylene glycol (¼, v/v) in the absence of an external field (B_{null}, Figure 5d). By advancing the magnet on the top of the device in the manner described in Figure 5a (B_{top}), the particles moved toward the magnet to exhibit the optically black sides of the MJPs on the top of the solution (Figure 5e). When

the magnet was moved to the bottom of the vessel (B_{bottom}), the particles switched their orientation to face their yellow sides toward the viewer (Figure 5f). While the "UM" letters comprising MJPs show a mixed color of yellow and black at B_{null} (Figure 5g), the letters turn black at B_{top} (Figure 5h) and yellow at B_{bottom} (Figure 5i).

3. Conclusions

Controlling large-area assemblies of anisotropic magnetic particles at higher concentrations can produce appealing colloidal collective effects, which are clearly distinct from those obtained with individual anisotropic particles.[9,14,18,30] This work as well as work by others[8–14] underline the requirement for uniform orientation and tunable packing densities of magnetic particles. Precisely controlled switchability and alignment of magnetic particles, such as the multicompartmental particles used in this study, will likely contribute to new research activities, e.g., the fabrication of metamaterials with interesting optical cloaking

properties.[31] However, much remains to be done. When considering novel methods for dynamic manipulation of surface characteristics, future work will need to be directed toward finetuning of magnetic properties of multicompartmental particles and to access a broader range of switchable orientations.

4. Experimental Section

Characterization: See Figure S1 in the Supporting Information for the micrographs corresponding to OM, SEM, TEM, and CLSM.

Magnetic Assembly and Reconfiguration: The as-prepared particles were collected and suspended in deionized (DI) water containing 0.1 wt% of Tween 20 (Sigma-Aldrich). The particle suspension (50 µL) was placed onto the one side of the glass slide containing the PLGA fibers, and then DI water (300 µL) was carefully loaded so that a layer of water was spread on the glass slide. This experimental setup was configured on the stage of the optical microscope. While maintaining the field direction perpendicular to the stage (the x–y-plane), the magnet ($1'' \times 1'' \times 1/2''$ thick, NdFeB, K&J Magnetics, Inc.) was placed close to the microscope. Once the alignment of the MJPs was confirmed by microscopy, the rotation of the magnet at a right angle induced the reconfiguration of the assembled particles depending on the field rotational directions, i.e., + or −90°.

Shape Transformation: The microcylinders were transformed into spherically shaped particles (≈450 µm in diameter) by applying a plasticizer, 1,4-dioxane, in a mixture of water and Tween 80 (2/1, v/v) until the particle shape changed from the cylinder to sphere (in general, the same volume ratio was used). An excess of water was added to the mixture to stop the transformation. The spherical particles were filtered using a membrane filter (45 µm) and washed with water.

Simulation Model: In Figure 2a, the green-red sphere represents the excluded volume of a particle. The black arrow indicates the location and orientation of the dipole vector with respect to the particle center of mass. It was assumed that the magnetite nanocrystals were homogeneously distributed throughout the red hemisphere, and thus the induced dipole moment was located at the center of mass of the red hemisphere. Similar assumptions for simulation models of magnetic particles with point dipoles embedded can be found elsewhere.[32–35] The distance between the black arrow and the particle center of mass was 0.1875σ, where σ is the particle diameter. In this model (see the Supporting Information for details), the micrometer-sized particles were subject to 1) excluded volume interactions with each other and the wall, 2) dipole–dipole interactions, 3) magnetic field, 4) drag forces, and 5) thermal noise. The fiber wall was modeled by a nonperiodic boundary along the x-direction. The excluded volume interaction was modeled by the Weeks–Chandler–Andersen potential,[36] which is commonly used for modeling such interactions between colloidal particles with the energy strength ε chosen so that the strongest magnetic force does not cause overlapping between particles under a strong field. Since the dynamics of the system in the presence of an external field plays a vital role in the formation of assembled structures, the order of magnitude of these relevant interactions were matched so that the dynamics in the model were consistent with those observed in the experiments. The dimensionless induced magnetic dipole is defined as

$$m = \frac{\mu}{k\sqrt{\sigma^3 \mu B}} \tag{2}$$

where k is a scaling factor of which the role is discussed in the Supporting Information. From the magnetization hysteresis of PLGA particles, it was determined that the particle dipole was in the order of $\mu = 10 \times 10^{-3}$ emu cm^{-3} × π (20 × 10^{-5} m)^3 = 10^{-14} A m^2. Since the strength of the applied gradient field was in the order of $B = 10^{-2}$ T, the field energy was $\mu B = 10^{-14}$ A m^2 × 10^{-2} T = 10^{-15} J, much greater than the thermal energy $k_B T$ at room temperature. μB was therefore chosen to be the energy scale. It was assumed that only the z component of the magnetic field B_z decreases linearly with the distance from a particle to the wall $B_z(x) = B_0 + ax$. Using the same force scale as for the dipole–dipole

interaction, $f = k^2 \mu_0 \mu B/(4\pi\sigma)$, the dimensionless gradient strength was defined as

$$g_B = \frac{4\pi a}{k\mu_0}\sqrt{\frac{\sigma^5}{\mu B}} \tag{3}$$

The fiber wall was modeled by a nonperiodic boundary along the x-direction.

For experimental conditions, $a = 1$ T m^{-1}, $\mu = 10^{-14}$ A m^2, $B = 10^{-2}$ T, F_c and F_b were ≈0.04 × 10^{-12} N, $F_d \approx 0.003 \times 10^{-12}$ N, and $F_v \approx 1.0 \times 10^{-12}$ N. F_b can be an order of magnitude greater than F_d to induce the directed assembly of the particles despite a relatively small value of the gradient strength (on the order of 1 T m^{-1}) compared to the particle diameter. $k = 10$, then $m \approx 1.0$, $g_B \approx 10.0$, was chosen so that the simulated value of $\varepsilon_{sim} \approx 1.0$, allowing the time unit in the simulation to be $\tau \approx 0.1$ s and the MD integration time step $\Delta t = 0.001\tau \approx 10^{-4}$ s (see below). As a result, the simulations were able to complete within 10^5–10^6 time steps.

Molecular dynamics was used to simulate a system of model PLGA particles in a thin slab in the z-direction. The particles were initialized randomly in the plane with a normal velocity distribution. The particles were then translated and rotated by integrating Newton's equations of motion using the velocity Verlet scheme. The particles were restricted between two nonattractive, impenetrable walls in the x-direction. Periodic boundary conditions were applied in the y-direction. To ensure that the resulting structures were reproducible, simulations were performed on different initial configurations with different random initial velocities. A typical system consists of $N = 100$–500 particles, and is equilibrated for 5×10^6–10×10^6 time steps until the final structure becomes stable. The natural units of the system are the particle diameter σ, the particle mass, the particle dipole magnitude m, and the magnetic field strength B. The simulations were performed with constant number of particles (N), constant volume (V), and constant temperature (T). As a validation of the model, it was possible to reproduce the well-known results for MJPs in homogeneous magnetic fields (comparing Figure S2 in the Supporting Information versus Figure 3). Simulations were performed using HOOMD-blue (http://glotzerlab.engin.umich.edu/hoomd-blue)[37] and LAMMPS (http://lammps.sandia.gov).[38]

Magnetophoretic Demonstrator: "UM" letters were drawn on the double-sided tape (3M) and silicone (1/16″ and 0.02″ thick, McMaster Carr), respectively, using SolidWorks DWGeditor software. The tape and silicone were cut by printing the drawings in a vector mode via Epilog Zing 16 Laser. After a piece of double-sided tape was laminated onto a glass slide (bottom of the device, 25 × 75 × 1 mm), the silicone treated with a high frequency generator (Electro-Technic Products, Inc., Model BD-20) was attached on top of the double-sided tape. In this manner, another double-sided tape and silicone were added until reaching to a desired height (2 or 4 mm). The prepared particles suspended in a mixture of Tween 80 and ethylene glycol (¼, v/v) were loaded into the given geometries in the device until the particles covered the surface. Another glass slide with the double-sided tape was sealed to the top of the device. Finally, the inside of the feature was fully filled with the medium by injecting through the wall of device using a syringe and needle. The letter dimension was 10 (length) × 2 (thickness of channel) × 4 (height) mm.

Supporting Information

Supporting Information is available from the Wiley Online Library or from the author.

Acknowledgements

[1] T. Kato, *Science* **2002**, *295*, 2414.
[2] J. W. Goodby, *Curr. Opin. Solid State Mater. Sci.* **1999**, *4*, 361.
[3] J. Lahann, S. Mitragotri, T. N. Tran, H. Kaido, J. Sundaram, I. S. Choi, S. Hoffer, G. A. Somorjai, R. Langer, *Science* **2003**, *299*, 371.
[4] Y. Y. Luk, N. L. Abbott, *Science* **2003**, *301*, 623.
[5] B. Comiskey, J. D. Albert, H. Yoshizawa, J. Jacobson, *Nature* **1998**, *394*, 253.
[6] T. Nisisako, T. Torii, T. Takahashi, Y. Takizawa, *Adv. Mater.* **2006**, *18*, 1152.
[7] A. Snezhko, *J. Phys.: Condens. Matter* **2011**, *23*, 153101.
[8] B. A. Grzybowski, K. Fitzner, J. Paczesny, S. Granick, *Chem. Soc. Rev.* **2017**, *46*, 5647.
[9] R. M. Erb, N. J. Jenness, R. L. Clark, B. B. Yellen, *Adv. Mater.* **2009**, *21*, 4825.
[10] J. Yan, M. Bloom, S. C. Bae, E. Luijten, S. Granick, *Nature* **2012**, *491*, 578.
[11] S. K. Smoukov, S. Gangwal, M. Marquez, O. D. Velev, *Soft Matter* **2009**, *5*, 1285.
[12] K. P. Yuet, D. K. Hwang, R. Haghgooie, P. S. Doyle, *Langmuir* **2009**, *26*, 4281.
[13] L. Zhang, F. Zhang, W.-F. Dong, J.-F. Song, Q.-S. Huo, H.-B. Sun, *Chem. Commun.* **2011**, *47*, 1225.
[14] S. Kim, J. Y. Sim, J. Lim, S. Yang, *Angew. Chem., Int. Ed.* **2010**, *49*, 3786.
[15] C. Chen, A. R. Abate, D. Lee, E. M. Terentjev, D. A. Weitz, *Adv. Mater.* **2009**, *21*, 3201.
[16] B. H. McNaughton, K. A. Kehbein, J. N. Anker, R. Kopelman, *J. Phys. Chem. B* **2006**, *110*, 18958.
[17] J. Yan, S. C. Bae, S. Granick, *Soft Matter* **2015**, *11*, 147.
[18] K.-H. Roh, D. C. Martin, J. Lahann, *Nat. Mater.* **2005**, *4*, 759.
[19] J. Yan, S. C. Bae, S. Granick, *Adv. Mater.* **2015**, *27*, 874.
[20] S. Bhaskar, K. M. Pollock, M. Yoshida, J. Lahann, *Small* **2010**, *6*, 404.
[21] K.-H. Roh, D. C. Martin, J. Lahann, *J. Am. Chem. Soc.* **2006**, *128*, 6796.
[22] J. Lahann, *Small* **2011**, *7*, 1149.
[23] S. Hwang, K.-H. Roh, D. W. Lim, G. Wang, C. Uher, J. Lahann, *Phys. Chem. Chem. Phys.* **2010**, *12*, 11894.
[24] T. O. Paine, L. I. Mendelsohn, F. E. Luborsky, *Phys. Rev.* **1955**, *100*, 1055.
[25] A. T. Skjeltorp, *Phys. Rev. Lett.* **1983**, *51*, 2306.
[26] J. Ge, J. Hu, T. Zhang, T. Huynh, Y. Yin, *Langmuir* **2008**, *24*, 3671.
[27] S. Rahmani, J. Lahann, *MRS Bull.* **2014**, *39*, 251.
[28] S. Bhaskar, J. Hitt, S. L. Chang, J. Lahann, *Angew. Chem., Int. Ed.* **2009**, *48*, 4589.
[29] K. J. Lee, J. Yoon, S. Rahmani, S. Hwang, S. Bhaskar, S. Mitragotri, J. Lahann, *Proc. Natl. Acad. Sci. USA* **2012**, *109*, 16057.
[30] S. Bhaskar, K. Roh, X. Jiang, G. L. Baker, J. Lahann, *Macromol. Rapid Commun.* **2008**, *29*, 1655.
[31] L. H. Gabrielli, J. Cardenas, C. B. Poitras, M. Lipson, *Nat. Photonics* **2009**, *3*, 461.
[32] J. J. Weis, *Mol. Phys.* **2002**, *100*, 579.
[33] A. Ghazali, J.-C. Lévy, *Phys. Rev. B* **2003**, *67*, 64409.
[34] M. Lattuada, T. A. Hatton, *J. Am. Chem. Soc.* **2007**, *129*, 12878.
[35] S. Kantorovich, R. Weeber, J. J. Cerdà, C. Holm, *J. Magn. Magn. Mater.* **2011**, *323*, 1269.
[36] J. D. Weeks, D. Chandler, H. C. Andersen, *J. Chem. Phys.* **1971**, *54*, 5237.
[37] J. A. Anderson, C. D. Lorenz, A. Travesset, *J. Comput. Phys.* **2008**, *227*, 5342.
[38] S. Plimpton, *J. Comput. Phys.* **1995**, *117*, 1.